

Full State Estimation of Soft Robots From Tip Velocities: A Cosserat-Theoretic Boundary Observer

Tongjia Zheng, Qing Han, and Hai Lin

Abstract—State estimation of robotic systems is essential to implementing feedback controllers which usually provide better robustness to modeling uncertainties than open-loop controllers. However, state estimation of soft robots is very challenging because soft robots have infinite degrees of freedom theoretically while existing sensors only provide a limited number of measurements. In this paper, we design an observer for soft robots based on the well-known Cosserat rod theory which models soft robots by nonlinear partial differential equations (PDEs). The observer is able to estimate all the continuous/infinite-dimensional robot states (poses, strains, and velocities) by only sensing the tip velocity of the robot (and hence it is called a “boundary” observer). More importantly, the estimation error dynamics is formally proven to be locally input-to-state stable. The key idea is to inject sequential tip velocity measurements into the observer in a way that dissipates the energy of the estimation errors through the boundary. Furthermore, this boundary observer can be implemented by simply changing a boundary condition in any numerical solvers of Cosserat rod models. Extensive numerical studies are included and suggest that the domain of attraction is large and the observer is robust to uncertainties of tip velocity measurements and model parameters.

Index Terms—Soft robots, continuum robots, Cosserat rod theory, state estimation

I. INTRODUCTION

Soft robotics is a rapidly growing area in the realm of robotics [1], [2]. Thanks to the compliant property of their materials, soft robots are safer when interacting with humans and are adaptable in constrained environments. As a result, soft robots have found many applications such as medical surgeries [3] and underwater maneuvers [4].

Despite the empirical evidence of their promising prospect, the theoretical study of soft robots has been considered a challenging problem, including aspects such as control, estimation, stability, and robustness. Many mathematical models, such as geometrical models, finite element models, and

continuum mechanics models, have been developed for soft robots [5], [6]. Geometrical models (especially piecewise constant curvature models) represent the deformed shape with a finite number of basis functions [7]. While early work has mainly focused on kinematic models, recent work has reported dynamic geometrical models in the form of under-actuated Lagrangian systems similar to those of rigid robot arms [8]. Finite element models represent the deformable shape as a large set of mesh nodes together with the information of their neighbors and usually rely on linearization and reduction for control design [9], [10]. Continuum mechanics models (especially Cosserat rod models) benefit from a physically rigorous definition of the kinetic and potential energy of the system and usually take the form of nonlinear PDEs [11], [12]. The dynamic geometrical models and finite element models may be viewed as finite-dimensional approximations of certain continuum mechanics models. Thus, continuum mechanics models are very promising in providing a rigorous theoretical framework for soft robots. However, since nonlinear PDEs are difficult to study, existing work has still relied on discretization to derive finite-dimensional Lagrangian representations [13], [14].

It is worth mentioning that most of the existing work is essentially based on discretization and can suffer from the trade-off between modeling accuracy and computational efficiency regarding the model complexity. This has motivated us to explore PDE control theory for soft robots. Recently, we reported a feedback controller directly based on an under-actuated Cosserat rod PDE without approximation [15]. The controller is proven to be stable and suggests the promising role of PDE control theory in soft robotics. As a feedback controller, however, it requires knowing all the continuous robot states, which motivates the state estimation problem in this work. Unlike traditional rigid-body robots, estimation of soft robots is very challenging because theoretically, soft robots have infinite degrees of freedom, while existing sensors can only provide a limited number of point measurements of their infinite-dimensional states.

Related work: The majority of existing work has focused on static estimation (or shape estimation), which assumes that the robot is in a quasi-static state and aims to estimate the configuration of the entire soft robot from point measurements of certain variables, such as position, orientation, and force. The common strategy is to fit an assumed static/time-independent model to the point measurements, such as a spatial curve [16],

*This work was supported by the National Science Foundation under Grant No. CNS-1830335, IIS-2007949.

Tongjia Zheng is with the Department of Electrical Engineering and the Department of Mathematics, University of Notre Dame, Notre Dame, IN 46556, USA. (tzheng1@nd.edu.)

Qing Han is with the Department of Mathematics, University of Notre Dame, Notre Dame, IN 46556, USA. (Qing.Han.7@nd.edu.)

Hai Lin is with the Department of Electrical Engineering, University of Notre Dame, Notre Dame, IN 46556, USA. (hlin1@nd.edu.)

[17] or a surface [18]. Physically more plausible solutions are those that fit a mechanical equilibrium to the measurements, such as a static Kirchhoff rod [19] or a static Cosserat rod [20]. The major limitation is the quasi-static assumption which ignores the robot dynamics. Dynamic estimation (or state estimation) is an iterative process that uses a dynamic model to predict new states and uses sequential sensor measurements to correct the prediction. Such an algorithm is referred to as an observer/filter. While dynamic PDE models based on continuum mechanics are available, existing work has mainly adopted their finite-dimensional approximations and designed extended Kalman filters (EKFs) for state estimation [21]–[23]. To the best of our knowledge, the only existing work based on PDE models is our previous work [24] where a PDE-based EKF is reported.

In summary, existing work has revealed several limitations. First, existing work has mainly relied on finite-dimensional approximations, which may introduce extra modeling uncertainty. Second, existing work typically requires a large number of sensors for good accuracy, which can be expensive and also damage the property of soft robots. Third, no result is available concerning the convergence of the estimation algorithms. This work is motivated to address these limitations.

Our contribution: In this work, we design a boundary observer for soft robots based on the well-known Cosserat rod theory. This boundary observer is able to estimate all the infinite-dimensional robot states, e.g., poses, strains, and velocities, using the PDE model, inputs, and only tip velocity measurements (which explains the name “boundary” observer). The key idea is to inject sequential tip velocity measurements into the observer in a way that dissipates the energy of state estimation errors through the boundary. It has three major advantages over the existing work.

- 1) It only requires sensing the tip velocity.
- 2) It can be implemented by changing a boundary condition in any numerical solvers of Cosserat rod models.
- 3) The state estimation error is proven to be locally input-to-state stable.

This is the first work that is able to construct a stable (PDE-based) observer for soft robots. To appreciate its significance, we point out that stability guarantee for nonlinear state estimation is rare even for finite-dimensional systems. Boundary estimation of PDEs is even harder due to the very limited amount of measurements as opposed to the amount of unknown states we want to estimate. In this regard, the stability guarantee provided in this work is a significant contribution. Numerical studies using SoRoSim [25], a MATLAB toolbox for soft robots, suggest that the domain of attraction is large and the observer is robust to uncertainties of tip measurements and model parameters. Together with our recent work on PDE-based control [15], it suggests the promising role of PDE control theory in the theoretical study of soft robots.

Organization: The rest of the paper is organized as follows. In Section II, we introduce the Cosserat rod model and the state estimation problem. In Section III, we design a boundary observer and prove its stability. In Section IV, we conduct a series of numerical experiments to validate the

performance and robustness of the boundary observer. Section V summarizes the contribution and points out future direction.

II. MODELING AND PROBLEM FORMULATION

A. Notations and Preliminaries

We will make use of some Lie group notations from [26]. Denote by $SO(3)$ the special orthogonal group (the group consisting of all 3-D rotation matrices) and by $so(3)$ its associated Lie algebra. Denote by $SE(3)$ the special Euclidean group and by $se(3)$ its associated Lie algebra. A hat \wedge at the superscript of a vector η defines a matrix η^\wedge whose definition depends on the dimension of η . Specifically, if $\eta \in \mathbb{R}^3$, then $\eta^\wedge \in so(3)$ is such that $\eta^\wedge \xi = \eta \times \xi$ for any $\xi \in \mathbb{R}^3$ where \times is the cross product. If $\eta = [w^T, v^T]^T \in \mathbb{R}^6$ with $w, v \in \mathbb{R}^3$, then $\eta^\wedge \in se(3)$ is defined by

$$\eta^\wedge = \begin{bmatrix} w^\wedge & v \\ 0 & 0 \end{bmatrix} \in \mathbb{R}^{4 \times 4}.$$

Let the superscript \vee be the inverse operator of \wedge , i.e., $(\eta^\wedge)^\vee = \eta$. The operator ad of $\eta = [w^T, v^T]^T \in \mathbb{R}^6$ with $w, v \in \mathbb{R}^3$ is defined by

$$ad_\eta = \begin{bmatrix} w^\wedge & 0 \\ v^\wedge & w^\wedge \end{bmatrix} \in \mathbb{R}^{6 \times 6}.$$

By definition, ad is a linear operator and satisfies $ad_\eta \xi = -ad_\xi \eta$ for $\xi, \eta \in \mathbb{R}^6$.

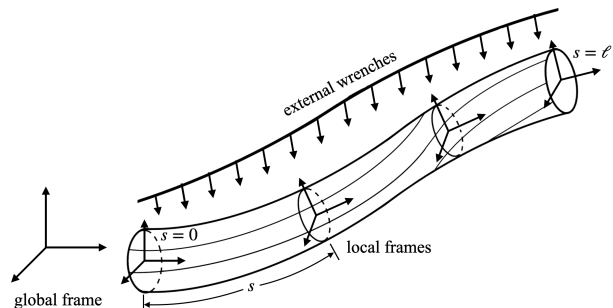


Fig. 1: A Cosserat rod.

B. Cosserat Rod Theory

Cosserat rod models are continuum mechanics models that describe the dynamic response of long and thin deformable rods undergoing external wrenches and have been widely used to model soft robots [11], [12], [15]. A Cosserat rod is idealized as a continuous set of rigid cross-sections stacked along a centerline parameterized by a material coordinate $s \in [0, \ell]$; see Fig. 1. Let $t \in [0, T]$ be the temporal coordinate. The pose of the entire rod is uniquely defined by a function $g(s, t) \in SE(3)$ given by

$$g = \begin{bmatrix} R & p \\ 0 & 1 \end{bmatrix},$$

where $p(s, t) \in \mathbb{R}^3$ is the position vector of the centerline and $R(s, t) \in SO(3)$ is the rotation matrix of the cross-sections.

Let $\eta = [w^T \ v^T]^T$ and $\xi = [u^T \ q^T]^T$ be the fields of velocity twists and strain twists, respectively, of the cross-sections in their local frames. The kinematics of the Cosserat rod is given by

$$\partial_t g = g \eta^\wedge, \quad (1)$$

$$\partial_s g = g \xi^\wedge, \quad (2)$$

where $\partial_t := \frac{\partial}{\partial t}$ and $\partial_s := \frac{\partial}{\partial s}$ are partial derivatives. The equality of mixed partial derivatives $\partial_{st}g = \partial_{ts}g$ yields the following compatibility equation between the strain and the velocity

$$\partial_t \xi = \partial_s \eta + ad_\xi \eta. \quad (3)$$

Let $\Phi = [m^T \ n^T]^T$ and $\Psi = [l^T \ f^T]^T$ be the fields of internal and external wrenches, respectively, of the cross-sections in their local frames. Let $\Psi_-(t)$ and $\Psi_+(t)$ be two tip external wrenches at $s = 0$ and $s = \ell$. Applying Hamilton's principle in the context of Lie groups yields the following dynamics of the Cosserat rod in the form of nonlinear PDEs

$$J \partial_t \eta - ad_\eta^T J \eta = \partial_s \Phi - ad_\xi^T \Phi + \Psi, \quad (4)$$

where $J \in \mathbb{R}^{6 \times 6}$ is the cross-sectional inertial matrix, and boundary conditions at $s = 0$ and $s = \ell$

$$\begin{aligned} \eta(0, t) = \eta_-(t), \quad \text{or} \quad \Phi(0, t) = -\Psi_-(t), \\ \text{and} \quad \eta(\ell, t) = \eta_+(t), \quad \text{or} \quad \Phi(\ell, t) = \Psi_+(t), \end{aligned}$$

depending on whether we impose motion constraints ($\eta_-(t)$ and $\eta_+(t)$) or wrench constraints ($\Psi_-(t)$ and $\Psi_+(t)$) at the tips. For generality, we assume

$$\Phi = \phi + \phi_l, \quad \Psi = \psi_l + R^T \psi_g, \quad (5)$$

where ϕ is the field of the elastic wrench which is assumed to satisfy the following linear constitutive law

$$\phi = K(\xi - \xi_*), \quad (6)$$

with $K \in \mathbb{R}^{6 \times 6}$ being the cross-sectional stiffness matrix and ξ_* being the strain field of the reference configuration, ϕ_l is the internal wrench applied by internal actuation (like pneumatic actuation), ψ_l is the portion of externally applied wrench whose value is specified in the local frames (like tendon actuation), and $R^T \psi_g$ is the portion whose value is specified by ψ_g in the global frame (like gravity) and converted to local frames by left-multiplying R^T . It is important to distinguish between ψ_l and $R^T \psi_g$ for state estimation problems because the rotation matrix R is also an unknown robot state.

Remark 1: A more general constitutive law with damping may be used to replace (6) by

$$\phi = K(\xi - \xi_*) + D \partial_t \xi, \quad (7)$$

where $D \in \mathbb{R}^{6 \times 6}$ is the damping matrix that models the viscoelastic property of the material. Our numerical study shows that the boundary observer to be presented later performs well in this case. However, from a theoretical perspective, (7) introduces mixed partial derivatives into the final PDE system, which makes it much harder to study its stability. Thus, all the theoretical results in this work are based on assuming a linear constitutive law (6).

C. Formulation of the Estimation Problem

This work is primarily interested in continuum manipulators. Thus, we assume the tip at $s = 0$ is clamped to a (static or mobile) station and the tip at $s = \ell$ is free or loaded. In this case, the following boundary conditions are applied

$$\eta(0, t) = \eta_-(t), \quad \Phi(\ell, t) = \Psi_+(t). \quad (8)$$

A minimum representation of the Cosserat rod model only requires two variables from the collection $\{g, \eta, \xi, \phi\}$ since the others can be correspondingly determined using (2) and (6) (or (7)). In our previous work [24], we chose $\{g, \eta\}$, assumed a linear constitutive law, and reported a PDE-based EKF. In this work, we mainly work with $\{\xi, \eta\}$ which satisfy the following PDE system

$$\begin{cases} \partial_t \xi = \partial_s \eta + ad_\xi \eta, \\ J \partial_t \eta = \partial_s(\phi + \phi_l) - ad_\xi^T(\phi + \phi_l) \\ \quad + ad_\eta^T J \eta + \psi_l + R^T \psi_g, \\ (\phi + \phi_l)(\ell, t) = \Psi_+(t), \\ \eta(0, t) = \eta_-(t), \\ \phi(s, 0) = \phi_0(s), \\ \eta(s, 0) = \eta_0(s), \end{cases} \quad (9)$$

where R and ϕ are determined by (2) and (6) (or (7)) respectively at every t , and $\{\eta_0, \phi_0\}$ are the initial conditions.

Assume the robot model (9), including its boundary conditions $\{\eta_-, \Psi_+\}$, and the distributed inputs $\{\phi_l, \psi_l, \psi_g\}$ are known. (The initial conditions are unknown.) Also assume that we can measure the tip velocity $\eta(\ell, t)$. This is called a boundary output/measurement and can be easily obtained by installing an initial measure unit (IMU) sensor at the tip. Our objective is to estimate the continuous/infinite-dimensional robot states $\{\xi, \eta\}$ based on the assumed information. Note that once this is done, one can compute estimates of other robot states $\{g, \phi\}$ using (2) and (6) (or (7)) at every t . The estimation problem of soft robots is stated as follows.

Problem 1 (Boundary Estimation): Given the soft robot model (9), its boundary conditions $\{\eta_-, \Psi_+\}$, distributed inputs $\{\phi_l, \psi_l, \psi_g\}$, and tip velocity measurements $\eta(\ell, t)$, design an algorithm to estimate the robot states $\{\xi, \eta\}$.

III. DESIGN AND STABILITY OF BOUNDARY OBSERVERS

For an unknown state variable, say η , we use a hat $\hat{\cdot}$ over the variable, i.e., $\hat{\eta}$, to denote its estimate. (We distinguish between $\hat{(\cdot)}$ and $(\cdot)^\wedge$ where the former is a state estimate while the latter is the hat operator defined in Section II-A.) Our estimation algorithm is called a boundary observer. The key idea is to inject the tip velocity measurement $\eta(\ell, t)$ into the observer in a way that dissipates the energy of state estimation errors through the boundary. The boundary observer is designed as

the following

$$\begin{cases} \partial_t \hat{\xi} = \partial_s \hat{\eta} + ad_{\hat{\xi}} \hat{\eta}, \\ J \partial_t \hat{\eta} = \partial_s (\hat{\phi} + \phi_l) - ad_{\hat{\xi}}^T (\hat{\phi} + \phi_l) \\ \quad + ad_{\hat{\eta}}^T J \hat{\eta} + \psi_l + \hat{R}^T \psi_g, \\ (\hat{\phi} + \phi_l)(\ell, t) = \Psi_+(t) - \Gamma(\hat{\eta} - \eta)(\ell, t), \\ \hat{\eta}(0, t) = \eta_-(t), \\ \hat{\phi}(s, 0) = \hat{\phi}_0(s), \\ \hat{\eta}(s, 0) = \hat{\eta}_0(s), \end{cases} \quad (10)$$

where $\Gamma \in \mathbb{R}^{6 \times 6}$ is a positive definite matrix representing the observer gain which can be used to adjust the performance of the observer, $\hat{\phi}$ is computed at every t using either

$$\hat{\phi} = K(\hat{\xi} - \xi_*) \quad (11)$$

according to (6), or

$$\hat{\phi} = K(\hat{\xi} - \xi_*) + D \partial_t \hat{\xi} \quad (12)$$

according to (7), \hat{R} is computed at every t using

$$\partial_s \hat{g} = \hat{g} \hat{\xi}^\wedge, \quad (13)$$

according to (2), which also produces estimates \hat{p} for the position, and $\{\hat{\phi}_0, \hat{\eta}_0\}$ are initial estimates.

This boundary observer has the classic observer structure in that it consists of a copy of the system plant plus injection of $(\hat{\eta} - \eta)(\ell, t)$, the prediction error of the tip velocity, through the boundary condition of $\hat{\phi}$. The injected term is designed in such a way that it dissipates the energy of the estimation errors, which will be more clearly observed when we arrive at the system of estimation errors (16). As a result, such a boundary condition is also called a dissipative boundary condition [27]. This boundary observer has three major advantages.

- 1) It only requires sensing the velocity of the free tip.
- 2) It can be implemented by changing a boundary condition in any numerical solvers of Cosserat rod models. In particular, the term $-\Gamma(\hat{\eta} - \eta)(\ell, t)$ can be implemented as a virtual point wrench at the tip.
- 3) The estimation error can be proven to be locally input-to-state stable (in the case of a linear constitutive law), which will be given in Theorem 1 shortly.

Remark 2: Since the observer eventually also needs to be numerically implemented based on discretization, one may wonder about the advantage of a PDE-based design as opposed to those directly based on discretized models. The answer is that PDE models are more compact and physically more interpretable. In fact, if one discretizes the PDE to obtain a large-scale ODE system, it will be very difficult (if not impossible) to observe that a simple technique of boundary dissipation can produce a stable nonlinear observer. Our recent work on PDE-based control of soft robots [15] uses energy dissipation to design stable controllers as well, which is also difficult to conceive if one discretizes the PDE in the first place.

From now on, we always assume a linear constitutive law, i.e., $D = 0$. To study the stability of the observer, define

$$\begin{aligned} \tilde{\phi} &= \hat{\phi} - \phi, & \tilde{\eta} &= \hat{\eta} - \eta, & \tilde{\xi} &= \hat{\xi} - \xi, & \tilde{R} &= \hat{R} - R, \\ y &= \begin{bmatrix} \phi \\ \eta \end{bmatrix}, & \hat{y} &= \begin{bmatrix} \hat{\phi} \\ \hat{\eta} \end{bmatrix}, & \tilde{y} &= \begin{bmatrix} \tilde{\phi} \\ \tilde{\eta} \end{bmatrix}, & d &= \begin{bmatrix} \phi_l \\ \psi_g \end{bmatrix}, \\ y_0 &= \begin{bmatrix} \phi_0 \\ \eta_0 \end{bmatrix}, & \hat{y}_0 &= \begin{bmatrix} \hat{\phi}_0 \\ \hat{\eta}_0 \end{bmatrix}, & \tilde{y}_0 &= \hat{y}_0 - y_0. \end{aligned}$$

By (6) and (11),

$$\tilde{\phi} = K \tilde{\xi}. \quad (14)$$

Subtracting (10) from (9), and by the linearity of ad and (14), we obtain that $\tilde{\phi}$ satisfies

$$\begin{aligned} K^{-1} \partial_t \tilde{\phi} &= \partial_t \tilde{\xi} \\ &= \partial_s \tilde{\eta} + ad_{\tilde{\xi}} \tilde{\eta} - ad_{\xi} \eta \\ &= \partial_s \tilde{\eta} + ad_{\tilde{\xi}} \tilde{\eta} - ad_{\xi} \eta - ad_{\xi} \tilde{\eta} \\ &\quad + ad_{\xi} \tilde{\eta} + ad_{\xi} \eta - ad_{\xi} \eta \\ &= \partial_s \tilde{\eta} + ad_{\tilde{\xi}} \tilde{\eta} + ad_{\xi} \tilde{\eta} + ad_{\xi} \eta \\ &= \partial_s \tilde{\eta} + ad_{K^{-1} \tilde{\phi}} \tilde{\eta} + ad_{(K^{-1} \phi + \xi_*)} \tilde{\eta} + ad_{\xi} \eta, \end{aligned}$$

and by a similar derivation, $\tilde{\eta}$ satisfies

$$\begin{aligned} J \partial_t \tilde{\eta} &= \partial_s \tilde{\phi} - ad_{\tilde{\xi}}^T \tilde{\phi} - ad_{\xi}^T \tilde{\phi} - ad_{\xi}^T (\phi + \phi_l) \\ &\quad + ad_{\tilde{\eta}}^T J \tilde{\eta} + ad_{\tilde{\eta}}^T J \tilde{\eta} + ad_{\tilde{\eta}}^T J \eta + (\hat{R} - R)^T \psi_g \\ &= \partial_s \tilde{\phi} - ad_{K^{-1} \tilde{\phi}}^T \tilde{\phi} + ad_{\tilde{\eta}}^T J \tilde{\eta} - ad_{(K^{-1} \phi + \xi_*)}^T \tilde{\phi} \\ &\quad - ad_{K^{-1} \tilde{\phi}}^T (\phi + \phi_l) + ad_{\tilde{\eta}}^T J \tilde{\eta} + ad_{\tilde{\eta}}^T J \eta + \hat{R}^T \psi_g, \end{aligned}$$

with boundary conditions

$$\tilde{\eta}(0, t) = 0, \quad \tilde{\phi}(\ell, t) = -\Gamma \tilde{\eta}(\ell, t).$$

The complete system of estimation errors can be written as a semilinear hyperbolic system given in (15). One may observe that the estimation error does not depend on the boundary conditions $\{\eta_-, \Psi_+\}$ and the locally applied external wrench ψ_l because they are completely compensated by the observer. By left-multiplying (15) with Λ^{-1} (defined in (15)), we rewrite it in the following compact form

$$\begin{cases} \partial_t \tilde{y} + A \partial_s \tilde{y} + B \tilde{y} = F(\tilde{y}) + G(y, \tilde{y}) + H(d, \tilde{R}, \tilde{y}), \\ \tilde{\phi}(\ell, t) = -\Gamma \tilde{\eta}(\ell, t), \\ \tilde{\eta}(0, t) = 0, \\ \tilde{y}(s, 0) = \tilde{y}_0(s), \end{cases} \quad (16)$$

where $A = \Lambda^{-1} \bar{A}$, $B = \Lambda^{-1} \bar{B}$, $F = \Lambda^{-1} \bar{F}$, $G = \Lambda^{-1} \bar{G}$, and $H = \Lambda^{-1} \bar{H}$. We observe that the boundary condition of $\tilde{\phi}$ behaves like a damping term that dissipates energy from the system (16) [27], which is the key to rendering stability.

In the following theorem, the notion of input-to-state stability is used to study the stability of (16). Unfamiliar readers are referred to [28], [29] for a detailed introduction. Roughly speaking, a system is input-to-state stable if its solution is bounded by a positive function of external inputs and if it converges asymptotically in the absence of inputs. In our case, we will treat y and d as external inputs/disturbances and establish that $\|\tilde{y}(\cdot, t)\|_{H^1}$ locally converges to a neighborhood

$$\begin{aligned}
& \underbrace{\begin{bmatrix} K^{-1} & 0 \\ 0 & J \end{bmatrix}}_{\Lambda} \partial_t \begin{bmatrix} \tilde{\phi} \\ \tilde{\eta} \end{bmatrix} + \underbrace{\begin{bmatrix} 0 & -I \\ -I & 0 \end{bmatrix}}_{\bar{A}} \partial_s \begin{bmatrix} \tilde{\phi} \\ \tilde{\eta} \end{bmatrix} + \underbrace{\begin{bmatrix} 0 & -ad_{\xi_*} \\ ad_{\xi_*}^T & 0 \end{bmatrix}}_{\bar{B}} \begin{bmatrix} \tilde{\phi} \\ \tilde{\eta} \end{bmatrix} \\
& = \underbrace{\begin{bmatrix} ad_{K^{-1}\tilde{\phi}}\tilde{\eta} \\ ad_{\tilde{\eta}}^T J \tilde{\eta} - ad_{K^{-1}\tilde{\phi}}^T \tilde{\phi} \end{bmatrix}}_{\bar{F}(\tilde{y})} + \underbrace{\begin{bmatrix} ad_{K^{-1}\tilde{\phi}}\tilde{\eta} + ad_{K^{-1}\tilde{\phi}}\tilde{\eta} \\ -ad_{K^{-1}\tilde{\phi}}^T \tilde{\phi} - ad_{K^{-1}\tilde{\phi}}\tilde{\phi} + ad_{\tilde{\eta}}^T J \tilde{\eta} + ad_{\tilde{\eta}}^T J \tilde{\eta} \end{bmatrix}}_{\bar{G}(y, \tilde{y})} + \underbrace{\begin{bmatrix} 0 \\ -ad_{K^{-1}\tilde{\phi}}\phi_l + \tilde{R}^T \psi_g \end{bmatrix}}_{\bar{H}(d, \tilde{R}, \tilde{y})}
\end{aligned} \tag{15}$$

bounded by a positive function of $\|y(\cdot, t)\|_{H^1}$ (the true robot states) and $\|d(\cdot, t)\|_H$ (the inputs including gravity)¹. The well-posedness of the PDE systems in this work has been studied in [30]. In the following theorem, we assume that its solution uniquely exists in the functional space $C^0([0, T]; H^1(0, \ell))$ which is consistent with the results in [30].

Theorem 1: Consider (16). If Γ is positive-definite, then the estimation error $\|\tilde{y}(\cdot, t)\|_{H^1}$ is locally input-to-state stable in the sense that there exist constants $\beta, \lambda, \delta, \kappa_1, \kappa_2, \gamma_1, \gamma_2 > 0$ such that for all $\|\tilde{y}(\cdot, t)\|_{H^1} < \delta$, $\|y(\cdot, t)\|_{H^1} < \gamma_1$, $\|d(\cdot, t)\|_H < \gamma_2$, and $t \geq 0$, the following holds:

$$\begin{aligned}
\|\tilde{y}(\cdot, t)\|_{H^1} &\leq \beta \|\tilde{y}(\cdot, 0)\|_{H^1} e^{-\lambda t} + \kappa_1 \sup_{0 \leq \tau \leq t} \|y(\cdot, \tau)\|_{H^1} \\
&\quad + \kappa_2 \sup_{0 \leq \tau \leq t} \|d(\cdot, \tau)\|_H.
\end{aligned} \tag{17}$$

Proof: The proof is included in the Appendix. ■

On the right-hand side of (17), the first term is due to the initial estimation error and decays exponentially. The last two terms are proportional to certain norms of the true states and the inputs and therefore are always bounded in practice. Even though the theoretical convergence is only local, numerical studies suggest that the domain of attraction is quite large.

In practice, the performance of this boundary observer may depend on the accuracy of three pieces of information: the robot model, the tip velocity measurements, and the inputs. While no model is perfectly correct, continuum mechanics models have been recognized to be very promising for soft robots. The measurement of tip velocity using, e.g., IMUs, can be noisy and pre-filtering is very likely needed. Knowing the wrench inputs requires establishing the relationship between the generated wrench and the direct actuation reading (like chamber pressure or tendon strength) using experiments and identification in advance. The theoretical study on the robustness with respect to uncertainties of these three pieces of information is left as future work. Nevertheless, extensive numerical studies on the robustness will be conducted in the next section.

IV. NUMERICAL STUDY

To validate the performance of the presented boundary observer, we conduct numerical experiments on SoRoSim [25], a MATLAB toolbox for soft robots based on the Cosserat rod theory. It implements the discretization algorithm introduced

¹For a function $f(s)$, its H^1 norm is defined by $\|f\|_{H^1} := (\int f^2 + f'^2 ds)^{1/2}$. For a function $f(s, t)$, we define $\|f(\cdot, t)\|_H := (\int f^2 + (\partial_s f)^2 + (\partial_t f)^2 ds)^{1/2}$. Roughly speaking, these norms include not only the function itself but also its partial derivatives.

in [14] and therefore can be used as numerical implementation of our boundary observer by simply modifying one boundary condition. In particular, it is implemented by adding a virtual point wrench $-\Gamma(\hat{\eta} - \eta)(\ell, t)$ at the free tip $s = \ell$.

Length	1m
Cross-section radius	0.06m
Density	10^3kg/m^3
Young's modulus	10^6N/m^2
Poisson's ratio	0.5
Material damping	0 (default) or $1.125 \times 10^4 \text{Pa}\cdot\text{s}$

TABLE I: Robot parameters.

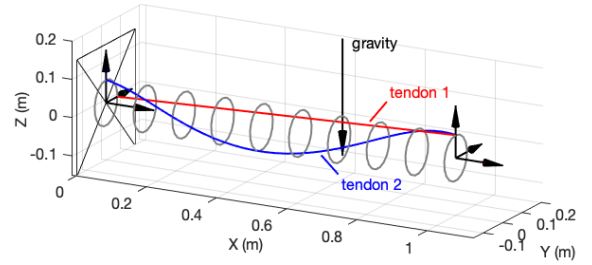


Fig. 2: A soft robot subject to gravity and tendon actuation.

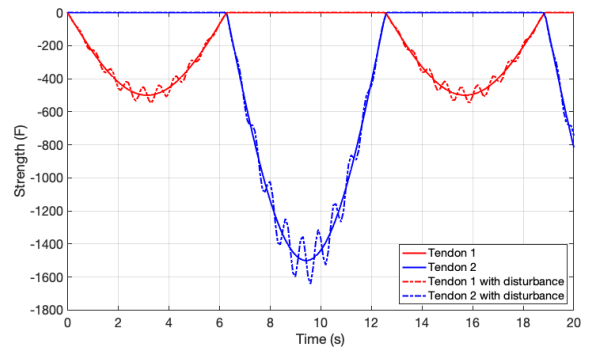


Fig. 3: Strengths of the tendons.

The robot parameters are given in Table I. The material damping is assumed to be 0 by default unless otherwise specified. The robot is subject to gravity and the actuation of two tendons; see Fig. 2. Tendon 1 is obliquely routed starting from $(x, y, z) = (0, 0.06, 0)$ to $(0, 0, 0.06)$. Tendon 2 is helically routed starting from $(x, y, z) = (0, 0, 0.06)$ and rotates with pitch = 0.16m/rad in a clockwise direction. The robot is initially at equilibrium which is a bending configuration due

to gravity. The two tendons are alternatively actuated to cause complicated 3D deformation of the robot. Their strengths are specified according to

$$\begin{aligned} T_1 &= -[500 \sin(t/2)]_+, \\ T_2 &= [1500 \sin(t/2)]_-, \end{aligned}$$

respectively, where f_+ and f_- represent the positive and negative parts of the function f ; see Fig. 3. In SoRoSim, all the strains are set to be active and approximated by polynomials of order 0. The order of the Gauss quadrature for numerical spatial integration is set to be 10. The MATLAB ODE solver ‘ode45’ is chosen for numerical temporal integration.

The sampling rate of the tip velocity is set to be 200Hz. A boundary observer (10) is used to estimate the robot states. The initial estimate is set to be a straight configuration, which has a large initial estimation error. A series of independent experiments are performed to study the impact of different factors, such as observer gains, velocity measurement uncertainty, model parameter uncertainty, actuation input uncertainty, and material damping.

A. Experiment 1: Impact of Observer Gains

This experiment is to validate the theoretical results and hence no uncertainty is added. To study the impact of different observer gains, we set $\Gamma = 0.2, 0.3, 0.4$.

Result. An illustration² of the estimation process is given in Fig. 4. We observe that the estimated configuration gradually converges to the true configuration. The L^∞ norms of estimation errors of all robot states are plotted in Fig. 5, which exhibit exponential convergence toward a small neighborhood of 0. This verifies the input-to-state stable property of the boundary observer. Moreover, larger observer gains always result in faster convergence. Although the theoretical results are only local, the large initial estimation errors suggest that the domain of attraction is large. The velocity estimates tend to have larger estimation errors than the strains and poses especially when the actuation switches to a different tendon. This is possibly because velocities are directly affected by the actuation and exhibit more sensitivity.

B. Experiment 2: Impact of Tip Measurement Uncertainty

The tip velocity measurements using, e.g., IMUs, usually contain disturbances. To study the robustness to measurement uncertainty of the tip velocities, we add two kinds of disturbance to the tip velocity measurements: noise and bias.

1) *Experiment 2.1:* At every t , temporally independent noise is drawn from a uniform distribution on the interval $[-20\%, 20\%]$ of the average magnitude of the tip linear (angular) velocity and then added to each component of the tip linear (angular) velocity measurements.

2) *Experiment 2.2:* For all t , a temporally constant bias of 20% of the average magnitude of the tip linear (angular) velocity is added to each component of the tip linear (angular) velocity measurements.

Result. The L^∞ norms of estimation errors of all robot states are plotted in Fig. 6. Comparing it with Fig. 5, we observe that disturbances on tip velocity measurements only induce a very small amount of extra steady-state errors, which suggests that the boundary observer is very robust to tip measurement uncertainty.

C. Experiment 3: Impact of Model Uncertainty

In practice, the robot parameters may not be known exactly. To study the robustness to model uncertainty, spatially independent noise is drawn from a uniform distribution on the interval $[-20\%, 20\%]$ once and then added to the stiffness and inertial matrices $K(s)$ and $J(s)$ as a temporally constant bias.

Result. The L^∞ norms of estimation errors of all robot states are plotted in Fig. 7. Comparing it with Fig. 5, we observe that model uncertainty induces a small amount of extra steady-state errors, especially on the strains and poses. Nevertheless, the boundary observer exhibits reasonable robustness to model uncertainty.

D. Experiment 4: Impact of Input Uncertainty

In practice, it may be difficult to determine the exact amount of wrench generated by the actuators. To study the robustness to input uncertainty, we use the following perturbed input signals for the boundary observer; see Fig. 3 for illustration.

$$\begin{aligned} T_1 &= -[500 \sin(t/2)(1 + 0.1 \sin(10t))]_+, \\ T_2 &= [1500 \sin(t/2)(1 + 0.1 \sin(10t))]_-. \end{aligned}$$

Result. The L^∞ norms of estimation errors of all robot states are plotted in Fig. 8. Comparing it with Fig. 5, we observe that uncertainty of input signals induces a moderate amount of extra steady-state errors on all robot states. This is not surprising because the central idea of the boundary observer is to dissipate energy from estimation errors while inaccurate input signals may induce extra energy into the estimation errors. Future work will study how to use additional sensing (like position measurements) to compensate for the input uncertainty.

E. Experiment 5: Impact of Material Damping

All the theoretical results in this work are based on assuming the linear constitutive law (6). This experiment is to validate that the presented boundary observer also works for the constitutive law with damping (7). We set the material damping to be $1.125 \times 10^4 \text{Pa}\cdot\text{s}$ and assume it is known. Correspondingly, we use (12) to compute $\hat{\phi}$ for the boundary observer.

Result. The L^∞ norms of estimation errors of all robot states are plotted in Fig. 9. Comparing it with Fig. 5, we observe that the boundary observer exhibits better performance in terms of faster convergence rates and smaller steady-state errors. This is possibly because material damping results in slower motions, reduces oscillations, and helps dissipating energy.

²An animation can be found at <https://sites.google.com/nd.edu/tongjia-zheng/research>

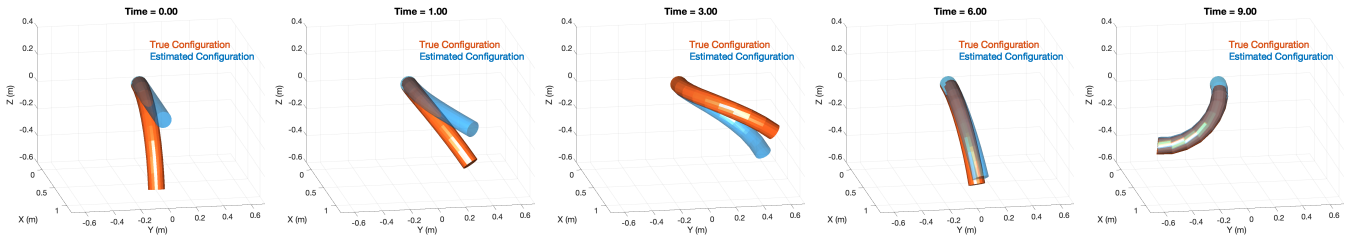


Fig. 4: Comparison of the true configuration (red) and estimated configuration (blue). ($\Gamma = 0.3$)

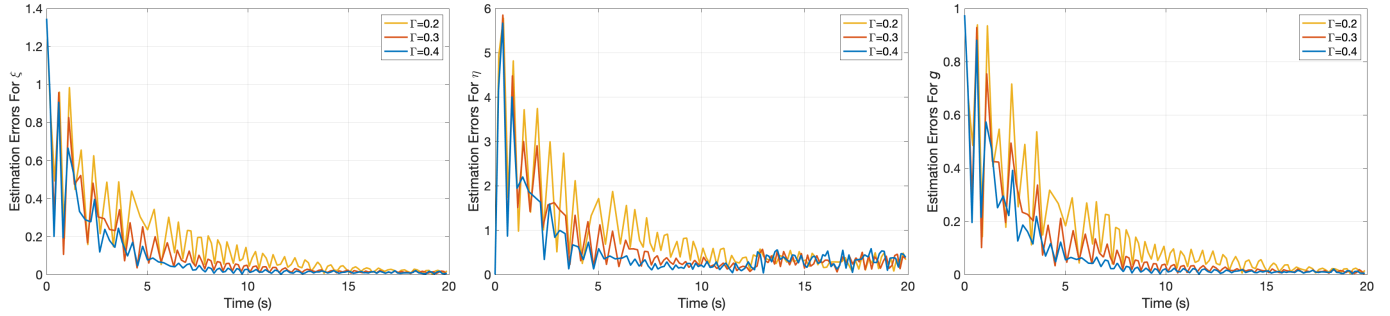


Fig. 5: Estimation errors (from left to right) $\|\tilde{\xi}(\cdot, t)\|_{L^\infty}$, $\|\tilde{\eta}(\cdot, t)\|_{L^\infty}$, and $\|\tilde{g}(\cdot, t)\|_{L^\infty}$ for Experiment 1 – Impact of Observer Gains. No uncertainty is added.

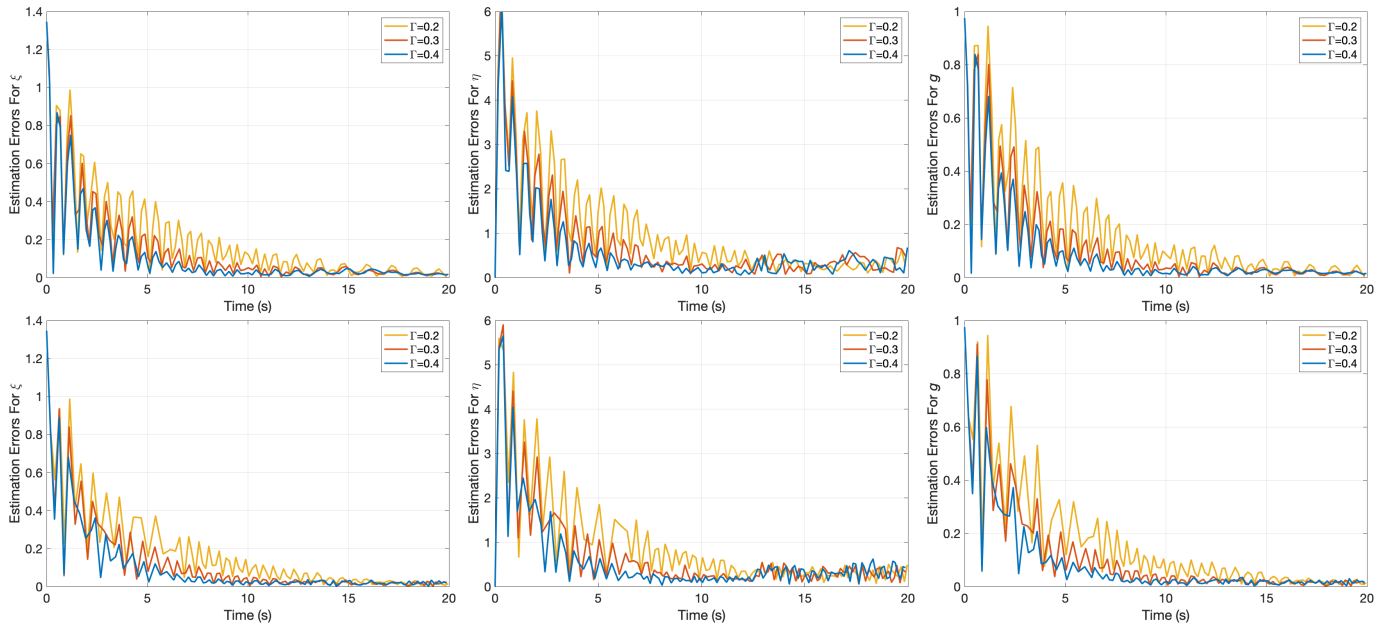


Fig. 6: Estimation errors (from left to right) $\|\tilde{\xi}(\cdot, t)\|_{L^\infty}$, $\|\tilde{\eta}(\cdot, t)\|_{L^\infty}$, and $\|\tilde{g}(\cdot, t)\|_{L^\infty}$ for Experiment 2 – Impact of Tip Measurement Uncertainty. Temporally independent measurement noise and a temporally constant measurement bias are added to the top and the bottom, respectively.

Remark 3: One can repeat Experiments 2-4 in the case when material damping is present and will find that similar robustness results also hold in this case.

F. Summary

In summary, although the theoretical stability is only local and requires a linear constitutive law, numerical studies suggest that the domain of attraction is large and the observer works well even with material damping. The observer turns out to be very robust to the tip measurement uncertainty,

followed by the model uncertainty, and is most sensitive to the uncertainty of input signals. Larger observer gains always result in faster convergence rates. However, this does not imply that a larger observer gain is always superior. In fact, in our numerical studies, a larger observer gain usually results in slower computation because it requires a smaller step size for temporal integration to ensure numerical stability.

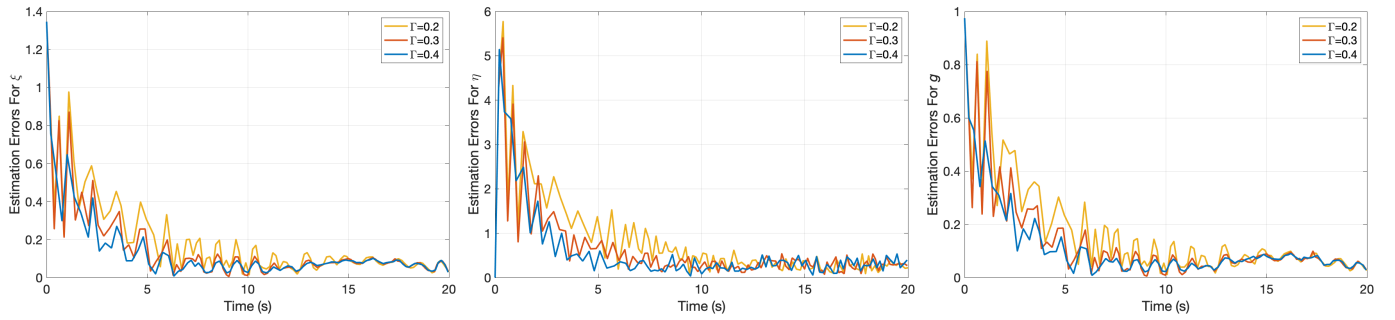


Fig. 7: Estimation errors (from left to right) $\|\tilde{\xi}(\cdot, t)\|_{L^\infty}$, $\|\tilde{\eta}(\cdot, t)\|_{L^\infty}$, and $\|\tilde{g}(\cdot, t)\|_{L^\infty}$ for Experiment 3 – Impact of Model Uncertainty. A spatially varying but temporally constant bias is added to the stiffness and inertial matrices.

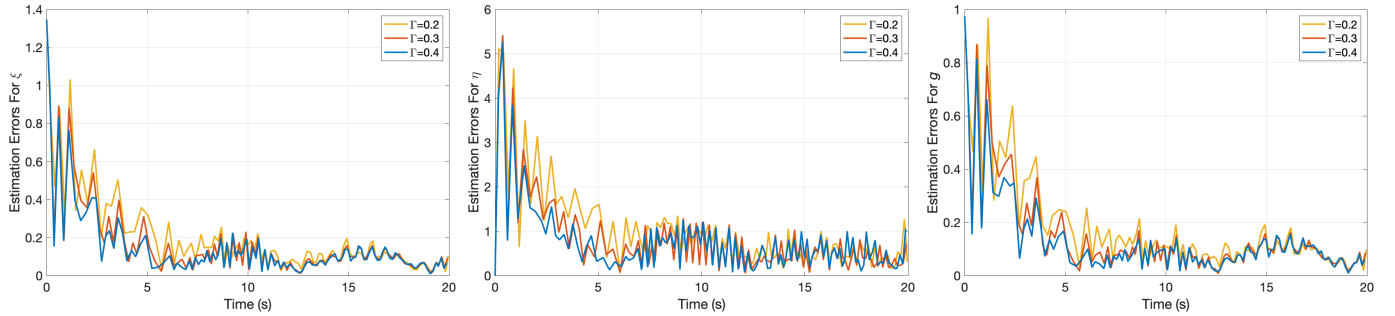


Fig. 8: Estimation errors (from left to right) $\|\tilde{\xi}(\cdot, t)\|_{L^\infty}$, $\|\tilde{\eta}(\cdot, t)\|_{L^\infty}$, and $\|\tilde{g}(\cdot, t)\|_{L^\infty}$ for Experiment 4 – Impact of Input Uncertainty. Disturbance is added to the wrench generated by the tendons.

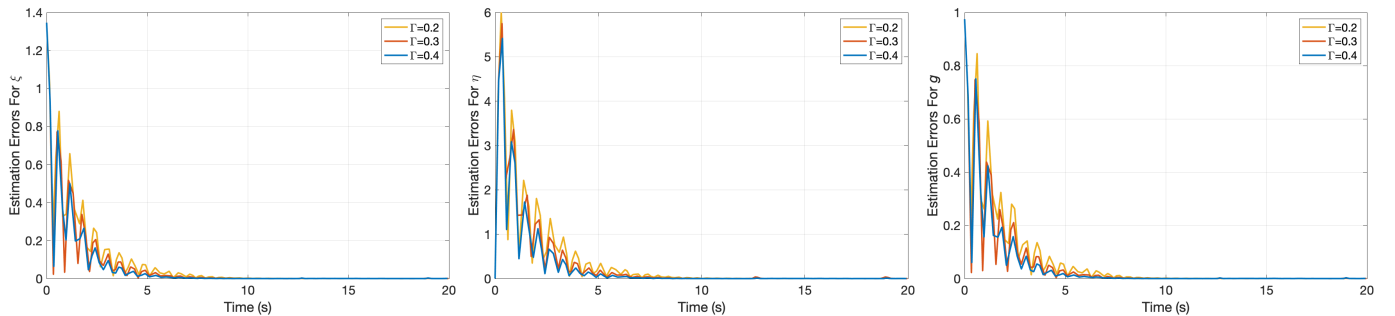


Fig. 9: Estimation errors (from left to right) $\|\tilde{\xi}(\cdot, t)\|_{L^\infty}$, $\|\tilde{\eta}(\cdot, t)\|_{L^\infty}$, and $\|\tilde{g}(\cdot, t)\|_{L^\infty}$ for Experiment 5 – Impact of Material Damping. A constitutive law with damping is adopted for both the robot and the observer.

V. CONCLUSION

In this work, we designed a boundary observer for soft robots based on Cosserat rod PDEs. This observer was able to estimate all continuous/infinite-dimensional robot states from only tip velocity measurements, could be easily implemented in both the hardware and numerical aspects, and was proven to be locally input-to-state stable. Extensive numerical experiments were conducted which suggested that the domain of attraction was large and the observer was robust to uncertainties of tip velocity measurements and model parameters. These results suggested the promising role of PDE control theory for soft robots. Our future work includes theoretical studies on the robustness of the observer, using additional sensing data to improve the robustness, and testing it on real platforms.

APPENDIX

A. Preliminaries for proving Theorem 1

The proof of Theorem 1 relies on some preliminary results from the work [30] which studies boundary stabilization of Cosserat rods. The main results are summarized here. Consider the following system with boundary control:

$$\begin{cases} \partial_t \xi = \partial_s \eta + ad_\xi \eta, \\ J \partial_t \eta = \partial_s \phi - ad_\xi^T \phi + ad_\eta^T J \eta, \\ \phi(\ell, t) = -\Gamma \eta(\ell, t), \\ \eta(0, t) = 0, \\ \phi(s, 0) = \phi_0(s), \\ \eta(s, 0) = \eta_0(s), \end{cases} \quad (18)$$

where $\Gamma \in \mathbb{R}^{6 \times 6}$ is the feedback gain. The system (18) is related to (9) by (i) setting all the inputs $\{\phi_l, \psi_l, \psi_g\}$ (including gravity) to be 0, (ii) setting the boundary condition

$\eta(0, t)$ to be 0, and (iii) setting the boundary condition $\phi(\ell, t)$ to be $-\Gamma\eta(\ell, t)$, which is the boundary controller in [30].

The total energy of (18), consisting of kinetic energy and (elastic) potential energy, is defined by

$$\mathcal{E}(t) = \int_0^\ell \eta^T J \eta + \phi^T K^{-1} \phi ds.$$

If $\Gamma = 0$, it is well-known that the total energy is conserved, i.e., $\frac{d}{dt}\mathcal{E}(t) = 0$. If $\Gamma > 0$, one can show that

$$\frac{d}{dt}\mathcal{E}(t) = -2\eta^T(\ell, t)\Gamma\eta(\ell, t) \leq 0,$$

which implies the total energy is non-increasing, i.e., (18) is stable. However, it is not necessarily decreasing, or asymptotically stable. The authors of [30] then managed to prove that (18) is locally exponentially stable by finding a modulated quadratic Lyapunov functional. In particular, (18) can be rewritten as

$$\begin{cases} \partial_t y + A\partial_s y + By = F(y) \\ \phi(\ell, t) = -\Gamma\eta(\ell, t), \\ \eta(0, t) = 0, \\ y(s, 0) = y_0(s), \end{cases} \quad (19)$$

where A , B , and F are defined in the same way as in (16). The following theorems summarize the main results from [30].

Theorem 2 (Well-posedness): For any $T > 0$, there exists $\delta > 0$ such that if y_0 satisfies $\|y_0\|_{H^1} \leq \delta$ and the compatibility conditions, then there exists a unique solution $y \in C^0([0, T], H^1)$ to (19). Moreover, if $\|y(\cdot, t)\|_{H^1} \leq \delta$ for all $t \in [0, T)$, then $T = +\infty$.

Theorem 3 (Local exponential stability): If Γ is positive-definite, then (19) is locally exponentially stable in H^1 . Moreover, a Lyapunov certificate is given by

$$\mathcal{V}(t) = \int_0^\ell y^T P y + \partial_t y^T P \partial_t y ds$$

where $P \in C^1([0, \ell]; \mathbb{R}^{12 \times 12})$ satisfies

- 1) $P(s)$ is positive-definite for all $s \in [0, \ell]$,
- 2) $(PA)(s)$ is symmetric for all $s \in [0, \ell]$,
- 3) $Q := -\frac{d}{ds}(PA) + PB + B^T P$ is positive-definite for all $s \in [0, \ell]$,
- 4) $(y^T P A y)(\ell, t) - (y^T P A y)(0, t) \geq 0$ for all t .

B. Proof of Theorem 1

Proof: By suitably renaming the variables, (16) can be seen as a perturbation of (19) with the injection of the nonlinear terms G and H . The main idea of our proof is to extend the original proof (in [30]) of Theorem 3 to accommodate the terms G and H and establish local input-to-state stability. Throughout the proof, all norms are defined only on the s variable and we also omit the dependence on t for brevity³.

³For instance, for a function $f(s, t)$, we denote $\|f\|_{L^2} = \|f(\cdot, t)\|_{L^2}$ which is actually a function of t but we omit t .

Let P satisfy all the properties in Theorem 3. Define Lyapunov functionals

$$\begin{aligned} \mathcal{V}_0(t) &= \int_0^\ell \tilde{y}^T P \tilde{y} ds, \\ \mathcal{V}_1(t) &= \int_0^\ell \partial_t \tilde{y}^T P \partial_t \tilde{y} ds. \end{aligned}$$

Let $\mathcal{V} = \mathcal{V}_0 + \mathcal{V}_1$. We will show that \mathcal{V} is equivalent to $\|\tilde{y}\|_{H^1}$ later in (25). Differentiating \mathcal{V}_0 , substituting (16), and then using integration by parts and the properties of P , we have

$$\begin{aligned} \dot{\mathcal{V}}_0 &= \int_0^\ell 2\tilde{y}^T P [-A\partial_s \tilde{y} - B\tilde{y} \\ &\quad + F(\tilde{y}) + G(y, \tilde{y}) + H(d, \tilde{R}, \tilde{y})] ds \\ &= -\tilde{y}^T P A \tilde{y} \Big|_0^\ell + \int_0^\ell \tilde{y}^T \partial_s (P A) \tilde{y} + \partial_s \tilde{y}^T P A \tilde{y} \\ &\quad - \tilde{y}^T P A \partial_s \tilde{y} - \tilde{y}^T P B \tilde{y} - \tilde{y}^T B^T P \tilde{y} \\ &\quad + \tilde{y}^T P [F(\tilde{y}) + G(y, \tilde{y}) + H(d, \tilde{R}, \tilde{y})] ds \\ &\leq \int_0^\ell -\tilde{y}^T Q \tilde{y} + \tilde{y}^T P [F(\tilde{y}) + G(y, \tilde{y}) + H(d, \tilde{R}, \tilde{y})] ds, \end{aligned}$$

where the term $\tilde{y}^T P A \tilde{y} \Big|_0^\ell \geq 0$ by the forth property of P and $Q := -\partial_s(PA) + PB + B^T P$ is positive-definite by the third property of P in Theorem 3. By a similar derivation,

$$\begin{aligned} \dot{\mathcal{V}}_1 &\leq \int_0^\ell -\partial_t \tilde{y}^T Q \partial_t \tilde{y} \\ &\quad + \partial_t \tilde{y}^T P \partial_t [F(\tilde{y}) + G(y, \tilde{y}) + H(d, \tilde{R}, \tilde{y})] ds. \end{aligned}$$

Thus, there exist a constant $C_0 > 0$ such that

$$\begin{aligned} \dot{\mathcal{V}} &\leq -C_0 \mathcal{V} + \sum_{i=0}^1 \int_0^\ell \partial_t^i \tilde{y}^T P \partial_t^i [F(\tilde{y}) \\ &\quad + G(y, \tilde{y}) + H(d, \tilde{R}, \tilde{y})] ds. \end{aligned} \quad (20)$$

Now we need to derive some estimates for the nonlinear terms F , G , and H . From now on, we assume there exist constants $\delta, \gamma_1, \gamma_2 > 0$ such that $\|\tilde{y}\|_{H^1} < \delta$, $\|y\|_{H^1} < \gamma_1$, and $\|d\|_H < \gamma_2$ for all t . By the Sobolev inequality [31], we correspondingly have $\|\tilde{y}\|_{L^\infty} < c_0 \delta$, $\|y\|_{L^\infty} < c_1 \gamma_1$, and $\|d\|_{L^\infty} < c_2 \gamma_2$ for some constants $c_0, c_1, c_2 > 0$.

By definition, $F(y)$ is a matrix-valued quadratic function consisting of only square terms. By Hölder's inequality [31], there exist constants $c_3, c_4 > 0$ such that

$$\begin{aligned} \int_0^\ell \tilde{y}^T P F(\tilde{y}) ds &\leq c_3 \|\tilde{y}\|_{L^\infty} \|\tilde{y}\|_{L^2}^2 \leq c_0 c_3 \delta \|\tilde{y}\|_{L^2}^2, \\ \int_0^\ell \partial_t \tilde{y}^T P \partial_t F(\tilde{y}) ds &\leq c_4 \|\tilde{y}\|_{L^\infty} \|\partial_t \tilde{y}\|_{L^2}^2 \leq c_0 c_4 \delta \|\partial_t \tilde{y}\|_{L^2}^2. \end{aligned}$$

The above estimates imply that there exists a constant $C_1 > 0$ such that

$$\sum_{i=0}^1 \int_0^\ell \partial_t^i \tilde{y}^T P \partial_t^i F(\tilde{y}) ds \leq C_1 \delta \mathcal{V}. \quad (21)$$

By definition, $G(y, \tilde{y})$ is a matrix-valued bilinear function. By Hölder's inequality, there exist constants $c_5, c_6, c_7 > 0$

such that

$$\begin{aligned} & \int_0^\ell \tilde{y}^T P G(y, \tilde{y}) ds \\ & \leq c_5 \|\tilde{y}\|_{L^\infty} \|\tilde{y}\|_{L^2} \|y\|_{L^2} \leq c_1 c_5 \delta \|\tilde{y}\|_{L^2} \|y\|_{L^2}, \\ & \int_0^\ell \partial_t \tilde{y}^T P \partial_t G(y, \tilde{y}) ds \\ & \leq c_6 \|\tilde{y}\|_{L^\infty} \|\partial_t \tilde{y}\|_{L^2} \|\partial_t y\|_{L^2} + c_7 \|y\|_{L^\infty} \|\partial_t \tilde{y}\|_{L^2}^2 \\ & \leq c_0 c_6 \delta \|\partial_t \tilde{y}\|_{L^2} \|\partial_t y\|_{L^2} + c_1 c_7 \gamma_1 \|\partial_t \tilde{y}\|_{L^2}^2. \end{aligned}$$

The above estimates, together with the fact that $\sum_{i=0}^1 \|\partial_t^i y\|_{L^2}$ is equivalent to $\|y\|_{H^1}$ ([30], p.p. 23), imply that there exist constants $C_2, C_3 > 0$ such that

$$\begin{aligned} & \sum_{i=0}^1 \int_0^\ell \partial_t^i \tilde{y}^T P \partial_t^i G(y, \tilde{y}) ds \\ & \leq C_2 \delta \sqrt{\mathcal{V}} \|y\|_{H^1} + C_3 \gamma_1 \mathcal{V}. \end{aligned} \quad (22)$$

According to the definition of \bar{H} in (15), we can denote $H(d, \tilde{R}, \tilde{y}) = H_1(d, \tilde{y}) + H_2(d, \tilde{R})$ where H_1 is the portion involving $ad_{K^{-1}\tilde{\phi}}\phi_I$ and H_2 is the portion involving $\tilde{R}^T \psi_g$. By definition, $H_1(d, \tilde{y})$ and $H_2(d, \tilde{R})$ are both matrix-valued bilinear functions. $H_1(d, \tilde{y})$ can be easily tackled in a similar way as $G(y, \tilde{y})$. In particular, we can deduce that there exist constants $C_4, C_5 > 0$ such that

$$\begin{aligned} & \sum_{i=0}^1 \int_0^\ell \partial_t^i \tilde{y}^T P \partial_t^i H_1(d, \tilde{y}) ds \\ & \leq C_4 \delta \sqrt{\mathcal{V}} \|d\|_H + C_5 \gamma_2 \mathcal{V}. \end{aligned} \quad (23)$$

Now we focus on $H_2(d, \tilde{R})$. According to (2), $\partial_s R = Ru^\wedge$ where u is the angular component of the strain ξ and therefore part of y . Since $\tilde{R}(0, t) = 0$ for all t , by the fundamental theorem of calculus, there exists a constant $c_8 > 0$ depending on ℓ such that

$$\begin{aligned} \|\tilde{R}\|_{L^\infty} & \leq c_8 \|\partial_s \tilde{R}\|_{L^\infty} \\ & = c_8 \|\hat{R} \hat{u}^\wedge - \hat{R} u^\wedge + \hat{R} u^\wedge - R u^\wedge\|_{L^\infty} \\ & \leq c_8 \|\hat{R} \hat{u}^\wedge\|_{L^\infty} + c_8 \|\tilde{R}\|_{L^\infty} \|u\|_{L^\infty} \\ & \leq c_9 \|\tilde{u}\|_{L^\infty} + c_1 c_8 \gamma_1 \|\tilde{R}\|_{L^\infty}, \end{aligned}$$

for some constant $c_9 > 0$, where we have used the fact that a rotation matrix \hat{R} has a bounded matrix norm. Thus, by choosing γ_1 to be sufficiently small, we have

$$\|\tilde{R}\|_{L^\infty} \leq \frac{c_9}{1 - c_1 c_8 \gamma_1} \|\tilde{u}\|_{L^\infty} =: c_{10} \|\tilde{y}\|_{L^\infty},$$

for some constant $c_{10} > 0$. By a similar argument as $\partial_s \tilde{R}$ and the fact that $\partial_t \tilde{R} = R w^\wedge$ where w is the angular component of the velocity η and therefore part of y , there exists a constant $c_{11} > 0$ such that

$$\begin{aligned} \|\partial_t \tilde{R}\|_{L^\infty} & \leq c_{11} \|\tilde{w}\|_{L^\infty} + c_1 \gamma_1 \|\tilde{R}\|_{L^\infty} \\ & \leq c_{11} \|\tilde{y}\|_{L^\infty} + c_1 c_{10} \gamma_1 \|\tilde{y}\|_{L^\infty} =: c_{12} \|\tilde{y}\|_{L^\infty}, \end{aligned}$$

for some constant $c_{12} > 0$. Now, by Hölder's inequality, there exist constants $c_{13}, c_{14} > 0$ such that

$$\begin{aligned} & \int_0^\ell \tilde{y}^T P H_2(d, \tilde{R}) ds \\ & \leq c_{13} \|\tilde{y}\|_{L^2} \|\tilde{R}\|_{L^\infty} \|\psi_g\|_{L^2} \leq c_0 c_{10} c_{13} \delta \|\tilde{y}\|_{L^2} \|\psi_g\|_{L^2}, \\ & \int_0^\ell \partial_t \tilde{y}^T P \partial_t H_2(d, \tilde{R}) ds \\ & \leq \int_0^\ell \partial_t \tilde{y}^T P [(\partial_t \tilde{R}^T) \psi_g + \tilde{R}^T \partial_t \psi_g] ds \\ & \leq c_{14} \|\partial_t \tilde{y}\|_{L^2} (\|\partial_t \tilde{R}\|_{L^\infty} \|\psi_g\|_{L^2} + \|\tilde{R}\|_{L^\infty} \|\partial_t \psi_g\|_{L^2}) \\ & \leq c_0 c_{14} \delta \|\partial_t \tilde{y}\|_{L^2} (c_{12} \|\psi_g\|_{L^2} + c_{10} \|\partial_t \psi_g\|_{L^2}). \end{aligned}$$

The above estimates imply that there exists a constant $C_6 > 0$ such that

$$\sum_{i=0}^1 \int_0^\ell \partial_t^i \tilde{y}^T P \partial_t^i H_2(d, \tilde{R}) ds \leq C_6 \delta \sqrt{\mathcal{V}} \|d\|_H. \quad (24)$$

We also need to show that \mathcal{V} is equivalent to $\|\tilde{y}\|_{H^1}$. Since the governing system of (16) is of first order in space and time, it yields a relationship between $\partial_t \tilde{y}$ and $\partial_s \tilde{y}$. In particular, using

$$\begin{aligned} \partial_t \tilde{y} & = -A \partial_s \tilde{y} - B \tilde{y} + F(\tilde{y}) + G(y, \tilde{y}) + H(d, \tilde{R}, \tilde{y}), \\ \partial_s \tilde{y} & = A^{-1} (-\partial_t \tilde{y} - B \tilde{y} + F(\tilde{y}) + G(y, \tilde{y}) + H(d, \tilde{R}, \tilde{y})), \end{aligned}$$

we can deduce that there exists a constant ϵ , depending on $A, B, \delta, \gamma_1, \gamma_2$, such that

$$\frac{1}{\epsilon} \sum_{i=0}^1 |\partial_s^i \tilde{y}|^2 \leq \sum_{i=0}^1 |\partial_t^i \tilde{y}|^2 \leq \epsilon \sum_{i=0}^1 |\partial_s^i \tilde{y}|^2, \quad (25)$$

which implies that \mathcal{V} and $\|\tilde{y}\|_{H^1}$ are equivalent. Thus, any stability results for \mathcal{V} implies similar results for $\|\tilde{y}\|_{H^1}$.

Now, using (20)-(24), we have

$$\begin{aligned} \dot{\mathcal{V}} & \leq -(C_0 - C_1 \delta - C_3 \gamma_1 - C_5 \gamma_2) \mathcal{V} \\ & \quad + \delta \sqrt{\mathcal{V}} (C_2 \|y\|_{H^1} + (C_4 + C_6) \|d\|_H) \\ & =: -C \mathcal{V} + \sqrt{\mathcal{V}} \mathcal{X}, \end{aligned}$$

where $C = C_0 - C_1 \delta - C_3 \gamma_1 - C_5 \gamma_2$ and $\mathcal{X} = \delta (C_2 \|y\|_{H^1} + (C_4 + C_6) \|d\|_H)$. We can let $\delta, \gamma_1, \gamma_2$ be sufficiently small such that $C > 0$. Let $\theta \in (0, 1)$ be a constant. Then whenever $\sqrt{\mathcal{V}} \geq \frac{1}{C\theta} \mathcal{X}$, we have

$$\begin{aligned} \dot{\mathcal{V}} & \leq -C(1 - \theta) \mathcal{V} - C\theta \mathcal{V} + \sqrt{\mathcal{V}} \mathcal{X} \\ & \leq -C(1 - \theta) \mathcal{V}. \end{aligned}$$

By invoking the Lyapunov function theorem for input-to-state stability [29], [32] and the equivalence of \mathcal{V} and $\|\tilde{y}\|_{H^1}$, we obtain the desired results. \blacksquare

REFERENCES

- [1] D. Rus and M. T. Tolley, "Design, fabrication and control of soft robots," *Nature*, vol. 521, no. 7553, pp. 467–475, 2015.
- [2] C. Laschi, B. Mazzolai, and M. Cianchetti, "Soft robotics: Technologies and systems pushing the boundaries of robot abilities," *Science robotics*, vol. 1, no. 1, p. eaah3690, 2016.

- [3] J. Burgner-Kahrs, D. C. Rucker, and H. Choset, "Continuum robots for medical applications: A survey," *IEEE Transactions on Robotics*, vol. 31, no. 6, pp. 1261–1280, 2015.
- [4] A. D. Marchese, C. D. Onal, and D. Rus, "Autonomous soft robotic fish capable of escape maneuvers using fluidic elastomer actuators," *Soft robotics*, vol. 1, no. 1, pp. 75–87, 2014.
- [5] C. Armanini, F. Boyer, A. T. Mathew, C. Duriez, and F. Renda, "Soft robots modeling: A structured overview," *IEEE Transactions on Robotics*, 2023.
- [6] C. Della Santina, C. Duriez, and D. Rus, "Model based control of soft robots: A survey of the state of the art and open challenges," *arXiv preprint arXiv:2110.01358*, 2021.
- [7] R. J. Webster III and B. A. Jones, "Design and kinematic modeling of constant curvature continuum robots: A review," *The International Journal of Robotics Research*, vol. 29, no. 13, pp. 1661–1683, 2010.
- [8] C. Della Santina, R. K. Katzschmann, A. Bicchi, and D. Rus, "Model-based dynamic feedback control of a planar soft robot: trajectory tracking and interaction with the environment," *The International Journal of Robotics Research*, vol. 39, no. 4, pp. 490–513, 2020.
- [9] C. Duriez, "Control of elastic soft robots based on real-time finite element method," in *2013 IEEE international conference on robotics and automation*. IEEE, 2013, pp. 3982–3987.
- [10] O. Gouy and C. Duriez, "Fast, generic, and reliable control and simulation of soft robots using model order reduction," *IEEE Transactions on Robotics*, vol. 34, no. 6, pp. 1565–1576, 2018.
- [11] D. C. Rucker and R. J. Webster III, "Statics and dynamics of continuum robots with general tendon routing and external loading," *IEEE Transactions on Robotics*, vol. 27, no. 6, pp. 1033–1044, 2011.
- [12] F. Renda, M. Giorelli, M. Calisti, M. Cianchetti, and C. Laschi, "Dynamic model of a multibending soft robot arm driven by cables," *IEEE Transactions on Robotics*, vol. 30, no. 5, pp. 1109–1122, 2014.
- [13] S. Grazioso, G. Di Gironimo, and B. Siciliano, "A geometrically exact model for soft continuum robots: The finite element deformation space formulation," *Soft robotics*, vol. 6, no. 6, pp. 790–811, 2019.
- [14] F. Boyer, V. Lebastard, F. Candelier, and F. Renda, "Dynamics of continuum and soft robots: A strain parameterization based approach," *IEEE Transactions on Robotics*, vol. 37, no. 3, pp. 847–863, 2020.
- [15] T. Zheng, Q. Han, and H. Lin, "Task space tracking of soft manipulators: Inner-outer loop control based on cosserat-rod models," in *to appear in 2022 American Control Conference (ACC)*, 2023.
- [16] D. Lunni, G. Giordano, E. Sinibaldi, M. Cianchetti, and B. Mazzolai, "Shape estimation based on kalman filtering: Towards fully soft proprioception," in *2018 IEEE International Conference on Soft Robotics (RoboSoft)*. IEEE, 2018, pp. 541–546.
- [17] H. Bezawada, C. Woods, and V. Vikas, "Shape reconstruction of soft manipulators using vision and imu feedback," *IEEE Robotics and Automation Letters*, vol. 7, no. 4, pp. 9589–9596, 2022.
- [18] R. B. Scharff, G. Fang, Y. Tian, J. Wu, J. M. Geraedts, and C. C. Wang, "Sensing and reconstruction of 3-d deformation on pneumatic soft robots," *IEEE/ASME Transactions on Mechatronics*, vol. 26, no. 4, pp. 1877–1885, 2021.
- [19] R. Takano, H. Mochiyama, and N. Takesue, "Real-time shape estimation of kirchhoff elastic rod based on force/torque sensor," in *2017 IEEE International Conference on Robotics and Automation (ICRA)*. IEEE, 2017, pp. 2508–2515.
- [20] S. H. Sadati, A. Shiva, N. Herzig, C. D. Rucker, H. Hauser, I. D. Walker, C. Bergeles, K. Althoefer, and T. Nanayakkara, "Stiffness imaging with a continuum appendage: Real-time shape and tip force estimation from base load readings," *IEEE Robotics and Automation Letters*, vol. 5, no. 2, pp. 2824–2831, 2020.
- [21] M. Thieffry, A. Kruszewski, C. Duriez, and T.-M. Guerra, "Control design for soft robots based on reduced-order model," *IEEE Robotics and Automation Letters*, vol. 4, no. 1, pp. 25–32, 2018.
- [22] J. Y. Loo, C. P. Tan, and S. G. Nurzaman, "H-infinity based extended kalman filter for state estimation in highly non-linear soft robotic system," in *2019 American Control Conference (ACC)*. IEEE, 2019, pp. 5154–5160.
- [23] K. Stewart, Z. Qiao, and W. Zhang, "State estimation and control with a robust extended kalman filter for a fabric soft robot," *IFAC-PapersOnLine*, vol. 55, no. 37, pp. 25–30, 2022.
- [24] T. Zheng and H. Lin, "Pde-based dynamic control and estimation of soft robotic arms," in *2022 IEEE 61st Conference on Decision and Control (CDC)*. IEEE, 2022, pp. 2702–2707.
- [25] A. T. Mathew, I. M. B. Hmida, C. Armanini, F. Boyer, and F. Renda, "Sorosim: A matlab toolbox for hybrid rigid-soft robots based on the geometric variable-strain approach," *IEEE Robotics & Automation Magazine*, 2022.
- [26] R. M. Murray, Z. Li, and S. S. Sastry, *A mathematical introduction to robotic manipulation*. CRC press, 2017.
- [27] G. Bastin and J.-M. Coron, *Stability and boundary stabilization of 1-d hyperbolic systems*. Springer, 2016, vol. 88.
- [28] H. K. Khalil and J. W. Grizzle, *Nonlinear systems*. Prentice hall Upper Saddle River, NJ, 2002, vol. 3.
- [29] S. Dashkovskiy and A. Mironchenko, "Input-to-state stability of infinite-dimensional control systems," *Mathematics of Control, Signals, and Systems*, vol. 25, no. 1, pp. 1–35, 2013.
- [30] C. Rodriguez, "Networks of geometrically exact beams: Well-posedness and stabilization," *Mathematical Control and Related Fields*, vol. 12, no. 1, pp. 49–80, 2022.
- [31] L. C. Evans, *Partial differential equations*, ser. Graduate Studies in Mathematics. Providence, RI: American Mathematical Society, 1998.
- [32] T. Zheng, Q. Han, and H. Lin, "Transporting robotic swarms via mean-field feedback control," *IEEE Transactions on Automatic Control*, vol. 67, no. 8, pp. 4170–4177, 2021.